Accepted Manuscript

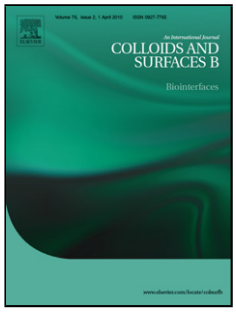

Title: Dual disassembly and biological evaluation of enzyme/oxidation-responsive polyester-based nanoparticulates for tumor-targeting delivery

Authors: Sung Hwa Hong, Kevin Larocque, Dilan B. Jaunky, Alisa Piekny, Jung Kwon Oh

PII: S0927-7765(18)30624-6
DOI: https://doi.org/10.1016/j.colsurfb.2018.09.013
Reference: COLSUB 9615

To appear in: *Colloids and Surfaces B: Biointerfaces*

Received date: 4-6-2018
Revised date: 27-8-2018
Accepted date: 5-9-2018

Please cite this article as: Hong SH, Larocque K, Jaunky DB, Piekny A, Kwon Oh J, Dual disassembly and biological evaluation of enzyme/oxidation-responsive polyester-based nanoparticulates for tumor-targeting delivery, *Colloids and Surfaces B: Biointerfaces* (2018), https://doi.org/10.1016/j.colsurfb.2018.09.013

Dual disassembly and biological evaluation of enzyme/oxidation-responsive polyester-based nanoparticulates for tumor-targeting delivery

Sung Hwa Hong, Kevin Larocque, Dilan B. Jaunky, Alisa Piekny, Jung Kwon Oh*

Department of Chemistry and Biochemistry, Concordia University, Montreal, Quebec, Canada H4B 1R6

Corresponding author: J.K.Oh (john.oh@concordia.ca)

Graphical abstract

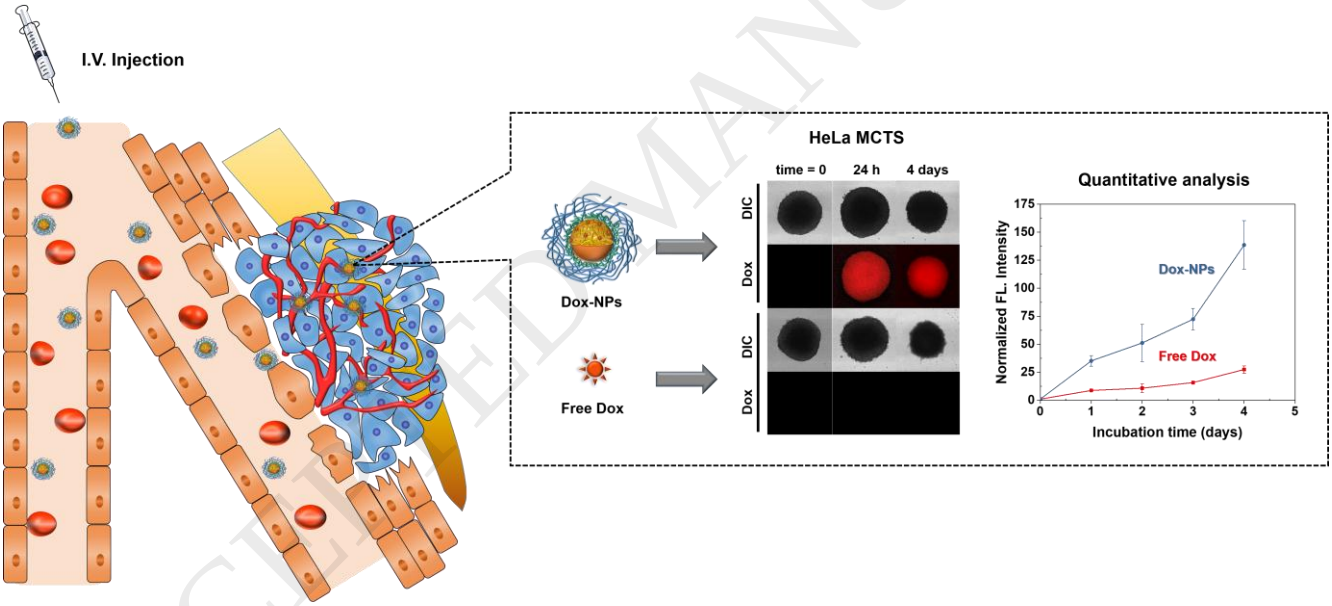

Highlights

- Versatility of dual responses to enzymatic and oxidative reactions
- Synthesis of polyester-based nanoparticles by a facile thiol-ene click reaction
- Rapid accumulation in tumor spheroids to inhibit tumor progression
- Cellular uptake of doxorubicin-loaded nanoparticles via caveolae-dependent mechanism

- Effective tumor-targeting intracellular nanocarriers

Abstract

Polyester-based nanoparticulates (NPs) are ideal nanocarriers for intracellular delivery of anticancer drugs because of their biocompatibility. However, an on-going challenge is the controlled and enhanced release of encapsulated therapeutics in response to unique changes that occur within cancer cells. Herein, we report the versatility of dual responses to enzymatic and oxidative reactions found in cancer cells toward the development of polyester-NPs as effective tumor-targeting intracellular nanocarriers. A facile nanoprecipitation method allows for the preparation of hydrophobic cores composed of novel polyester designed with esterase-responsive ester groups and oxidation-responsive sulfide linkages on their backbones, physically stabilized with poly(ethylene glycol)-based polymeric shells. The formed core/shell-type NPs with a diameter of 120 nm exhibit excellent colloidal stability in physiological conditions and in the presence of serum proteins. When exposed to esterase and hydrogen peroxide, NP integrity is disrupted, leading to the enhanced release of encapsulated doxorubicin, confirmed by dynamic light scattering and spectroscopic analysis. Combined results from epifluorescence microscopy, confocal laser scanning microscopy, flow cytometry, and cell viability demonstrate that doxorubicin-loaded NPs reveals rapid penetration and enhanced intracellular release of doxorubicin, thus inhibiting tumor progression. Importantly, the cellular uptake of doxorubicin-loaded core/shell NPs primarily via caveolae-dependent mechanism promotes their use in targeting a broad spectrum of cancers.

Keywords: ROS, esterase, dual stimuli-responsive degradation, polyester nanoparticles, controlled release, enhanced penetration, drug delivery

Introduction

Cancer is one of the leading causes of death worldwide, and tremendous resources have been devoted to develop anticancer therapies over the past few decades. Small molecule anticancer drugs, while having been used as effective chemotherapeutics, typically are not selective to cancer cells, and thus cause severe side effects. Further, high doses of drugs must be administered to overcome issues with solubility, metabolic reactivity, and/or poor efficacy due to their elimination by kidney filtration (or renal clearance) during blood circulation.[1-3] Recent efforts have shifted toward the development of methods that allow for the controlled delivery and release of small molecule anticancer drugs to improve their efficacy. Polymer-based drug delivery systems (PDDS),[4-7] particularly hydrophobic nanoparticulates,[8-10] possess a number of desirable properties such as biodegradability and

biocompatibility as well as ability to encapsulate therapeutic agents and deliver them to tumor tissues. Upon intravenous injection, well-designed PDDS with excellent colloidal stability have prolonged blood circulation; thus offering improved pharmacokinetics and biodistribution to tumors *via* enhanced permeability and retention (EPR).[11-13] Followed by their endocytosis into cancer cells, drug-loaded PDDS are subjected to the release of encapsulated drugs inside cells, thus minimizing side effects and maximizing therapeutic efficacy common to small molecule anticancer drugs. However, conventionally-designed PDDS remain a challenge to the controlled release of encapsulated drugs in the targeted cells.

Stimuli-responsive degradation (SRD) has been explored as a promising platform in the design of smart PDDS. SRD involves the incorporation of dynamic covalent linkages into the design of PDDS; when needed, the response of these linkages to external stimuli changes their chemical and physical properties. In such, SRD-exhibiting PDDS, which are stable under physiological conditions, can be dissociated in a controlled fashion as cellular components are provided appropriate stimuli, thus enabling biodegradation.[14-18] Acidic pH, glutathione, reactive oxygen species (ROS), and enzymatic activities are typical examples of endogenous stimuli, while light and temperature are exogenous stimuli.[19-21] The response to these stimuli has led to more precise control over the dissociation or disintegration of smart PDDS.[22-24] In particular, enzyme-responsive systems are especially promising in that enzymes are great catalysts with high selectivity towards specific substrates. Overexpressed disease-associated enzymes such as esterase are effective cellular triggers.[25, 26] With growing interest in enzyme-responsive platform, numerous PDDS have been designed with specific peptide linkages[27-32] or backbone ester or amide linkages.[33-37] In addition to esterase, ROS such as hydrogen peroxide, superoxide, hydroxyl radical, and hypochlorite is found at elevated concentrations in cancer cells compared to healthy cells.[38, 39] Most ROS-responsive systems have been designed to degrade as a consequence of a change in hydrophobic/hydrophilic balance of typically thioester (or sulfide) groups[40-42] or a cleavage of ROS-responsive phenylboronic ester groups[43, 44] upon oxidation. Although these advances with single response to either esterase or ROS, dual enzyme/oxidation-responsive systems has not been reported yet to our best knowledge.

In this work, we have explored dual enzyme/oxidation-responsive degradation of polyester-based nanoparticlulates (DPE-NPs) for tumor-targeting intracellular delivery exhibiting enhanced/controlled release of anticancer drugs (Figure 1). Hydrophobic DPE designed with both esterase-responsive ester bonds and oxidation-responsive sulfide linkages on the backbones was synthesized by a click-type

thiol-ene addition. A facile nanoprecipitation process of DPE with an aid of external polymeric stabilizers in water resulted in the fabrication of aqueous core/shell-type DPE NPs loaded with anticancer drugs. Polymeric shell composed of poly(ethylene oxide) provides stealth effect to minimize immune response and maximize colloidal stability in the blood. Porcine liver esterase and hydrogen peroxide were examined to model the response of DPE-NPs to esterase and ROS. Responses of DPE-NPs to these stimuli resulted in main chain degradation or polarity change, leading to the enhanced release of encapsulated doxorubicin (Dox) or hydrophobic model drug (Nile Red). Further, aqueous DPE-NPs were assessed as intracellular nanocarriers *in vitro* in two-dimensional (2D) monolayer cell culture and three-dimensional (3D) multicellular tumor spheroids (MCTS).

Experimental

Instrumentation. ^{1}H-NMR spectra were recorded using a 500 MHz Varian spectrometer. The $CDCl_3$ singlet at 7.26 ppm was selected as the reference standard. Molecular weight and molecular weight distribution were determined by gel permeation chromatography (GPC). An Agilent GPC was equipped with a 1260 Infinity Isocratic Pump and a RI detector. Two Agilent PLgel mixed-C and mixed-D columns were used with DMF containing 0.1 mol% LiBr at 50 °C at a flow rate of 1.0 mL/min. Linear poly(methyl methacrylate) standards from Fluka were used for calibration. Aliquots of the polymer samples were dissolved in DMF/LiBr. The clear solutions were filtered using a 0.45 μm PTFE filter to remove any solvent-insoluble species. A drop of anisole was added as a flow rate marker. The size of DPE-NPs in hydrodynamic diameter was measured by dynamic light scattering (DLS) at a fixed scattering angle of 175° at 25 °C with a Malvern Instruments Nano S ZEN1600 equipped with a 633 nm He-Ne gas laser. Fluorescence spectra on a Varian Cary Eclipse Fluorescence spectrometer and UV/Vis spectra on an Agilent Cary 60 UV/Vis spectrometer were recorded using a 1 cm wide quartz cuvette.

Transmission Electron Microscopy (TEM) images were obtained using a Philips Tecnai 12 TEM, operated at 80kV and equipped with a thermionic LaB6 filament. An AMT V601 DVC camera with point to point resolution and line resolution of 0.34 nm and 0.20 nm respectively was used to capture images at 2048 by 2048 pixels. To prepare specimens, the NP dispersions were dropped onto copper TEM grids (400 mesh, carbon coated), blotted and allowed to air dry at room temperature. Subsequently, uranyl acetate (1%) was applied on the TEM grids and then dried again at room temperature. The sizes in diameter of NPs were calculated using Image J software.

Microscope Imaging. Two types of microscopes were used. First, HeLa cells and multi-cellular tumor spheroid (HeLa and A549) were visualized with Nikon TI-E microscope equipped with LED Heliophors with a Photometrics Evolve EMCCD camera. Secondly, endocytosis mechanism of Dox-NPs was determined by using inverted Nikon Ti-E Livescan confocal microscope (CLSM) equipped with laser source (405 nm and 488 nm), a piezo Z stage (Mad City Labs), iXON897 EMCCD camera (Andor). NIS Elements acquisition software was used for both the microscopes. All the images were analyzed using Image J (NIH).

Materials. 2,2'-(ethylenedioxy)diethanethiol (DSH, 95%), ethylene glycol dimethacrylate (EGDMA, 98%), triethylamine (Et_3N, ≥99%), Brij® S20 (B20), poly(ethylene glycol) (PEG, MW = 6,000 g/mol), esterase from porcine liver (18 U/mg; one unit will hydrolyze 1 μmol of ethyl butyrate to butyric acid and ethanol per minute at pH 8.0 at 25 ºC), Nile Red (NR), doxorubicin hydrochloride (Dox, $-NH_3^+Cl^-$ forms, >98%), hydrogen peroxide (30% w/w), Bovine Serum Albumin (BSA), and Immunoglobulin G (IgG) from human serum (≥95%) from Aldrich, Pierce BCA protein assay kit from Bio-Rad, dialysis tubing from Spectrum Labs were purchased and used as received. Dulbecco's modified eagle medium (DMEM), F12K medium, and fetal bovine serum (FBS) from Wisent, phenol-red free DMEM from Thermo Fisher Scientific and 3-(4,5-dimethylthiazol-2-yl)-2,5-diphenyltetrazolium bromide (MTT) from Promega, and Hoescht 33342 from Invitrogen were purchased and used for biological assessment *in vitro*.

Synthesis of DPE. DSH (3.7 g, 20.2 mmol) was added to a solution consisting of EGDMA (4.0 g, 20.2 mmol) and Et_3N (565 μL, 4.0 mmol) dissolved in DMSO (13.5 mL) to start polymerization. The reaction mixture was stirred at room temperature for 24 hrs. The as-synthesized solution was precipitated from cold methanol to remove excess Et_3N and unreacted monomers. The precipitate was isolated by a vacuum filtration and dried in a vacuum oven at room temperature for 12 hrs, prior to analysis by ^1H NMR in $CDCl_3$ and by GPC.

Stabilizer-assisted NP formation by solvent evaporation method. An organic solution of the purified and dried DPE (10.8 mg) dissolved in THF (2.3 mL) was mixed with an aqueous solution of PEG (10.7 mg) and B20 (0.1 mg) in water (13.6 mL). The resulting dispersion was homogenized using sonifier (Branson) for 5 min (amplitude = 15 %, 10 sec on, 2.5 sec off) and then kept stirred for 24 hrs at room temperature to remove residual THF. A stable NP dispersion was formed at 2.0 mg/mL. The resulting mixtures, after being sonified, were purified by dialysis with MWCO = 12,000.

Enzyme/oxidative degradation of NPs. For oxidation-responsive degradation of NPs in the presence of hydrogen peroxide, aliquots of aqueous NP dispersion (2.0 mg/mL, 2.3 mL) were incubated with 1% v/v hydrogen peroxide under stirring at room temperature. For enzymatic degradation in the presence of esterase, aliquots of aqueous NP dispersion (2.0 mg/mL, 1.8 mL) were incubated with esterase (1 mg), attaining 10 U. Alternatively, the dispersion was incubated with esterase (2 mg) to attain 20 U. DLS was used to follow any changes in size distribution.

Preparation of Dox-loaded NPs (Dox-NPs). An organic solution containing DPE (12 mg), Dox (1 mg), and Et_3N (3.5 µL) dissolved in THF (2.8 mL) was mixed with an aqueous solution of B20 (0.6 mg) and PEG (11.5 mg) in water (11.7 mL). The resulting mixtures were homogenized using a sonifer (Branson) for 5 min (amplitude = 15 %, 10 sec on, 2.5 sec off) and stirred for 24 hrs to remove THF. They were then dialyzed over water (1 L) for 6 hrs to remove excess (free) Dox and Et_3N, yielding aqueous Dox-NPs at 2.0 mg/mL. First, the extinction coefficient of Dox was determined in a mixture of water/THF (1/4 v/v) using a UV/vis spectroscopy along with Beer-Lambert equation. Then, the loading level and loading efficiency of Dox were determined with mixtures consisting of aliquots of Dox-NPs (1 mL) mixed with THF (4 mL). The UV/vis spectra were recorded to obtain the absorbance at 498 nm.

Colloidal stability in the presence of proteins. Aqueous DPE NP dispersion (1 mL, 2 mg/mL) was divided into two aliquots and was mixed with BSA (1 mL, 80 mg/mL) and IgG (1 mL, 16 mg/mL) in PBS. As controls, BSA and IgG solutions were prepared at the same concentrations. The mixtures were incubated at 37 °C for 48 hrs. Aliquots from each mixture were withdrawn and subjected to centrifugation (10,000 rpm x 15 min) to precipitate undesirably-formed aggregates. The supernatants were quantitatively analyzed using BCA assays according to the Pierce® BCA assay kit instructions. Briefly, supernatant (25 µL) was transferred to a 96-well plate and BCA reagent (200 µL) was added to each well. The plate was then placed at 37 °C for 30 min and the absorbance was measured at λ = 562 nm using Powerwave HT Microplate Reader (Bio-Tek). Percentage of free protein was calculated by the ratio of the absorbance with NPs to that without NPs (control).

Esterase-triggered release of Dox from Dox-NPs. An aqueous mixture consisting of an esterase stock solution (0.24 mL, 2.6 mg/mL) and a Dox-NP dispersion (0.9 mL, 5.1 mg/mL) in PBS was transferred into dialysis tubing (MWCO = 12,000 g/mol) and immersed in PBS (40 mL). The UV spectrum of Dox in outer water was recorded at indicated time intervals using a UV/Vis spectrometer. For quantitative analysis, Dox (94.8 µg, equivalent to Dox encapsulated in 0.9 mL Dox-NPs) was dissolved in PBS to record its UV/Vis spectrum.

Degradation of Dox upon oxidation. Dox (0.15 mg) was dissolved in 1% v/v (or 323 mM) hydrogen peroxide solution in water (5 mL). Aliquots taken periodically were analyzed by UV/vis spectroscopy to follow the absorbance at 498 nm.

Oxidation-responsive release of NR from aqueous NR-loaded NPs. First, aqueous NR-loaded NPs were prepared as follows; an aqueous stabilizer solution (B20/PEG = 0.05 w/w, 1.1 mg/mL, 10.5 mL) was mixed with an organic solution consisting of NR (0.9 mg) and DPE (11 mg) in THF (2.4 mL). The resulting mixture was homogenized for 5 min and stirred for 24 hrs to remove THF, followed by filtration using 0.85 μm PES filter (Pall Corporation) to remove free NR. Then, aliquots of NR-loaded NPs were mixed with hydrogen peroxide (1% and 5% v/v) while stirring at 37 ºC. Their fluorescence spectra (λ_{ex} = 480 nm) were recorded periodically to follow FL intensity at 620 nm.

Cell culture. HeLa cervical cancer cells were cultured in DMEM (Dulbecco's modified Eagle's medium) containing 10% FBS (fetal bovine serum) and 1% antibiotics (50 units/mL penicillin and 50 units/mL streptomycin) at 37 °C in a humidified atmosphere containing 5% CO_2. A549 cells were cultured in F12K media with same supplemental additives as previously mentioned; 10% FBS and 1% antibiotics.

Cell viability using MTT assay. HeLa cells were plated at 5 x 10^5 cells per well into a 96-well plate and incubated for 24 h in DMEM (100 μL) containing 10 % FBS and 1 % antibiotics. Then, they were incubated with various concentrations of empty (Dox-free), free Dox, and Dox-NPs for 48 h. Blank controls without nanoparticles (cells only) were run simultaneously as control. Cell viability was measured using the CellTiter 96 Non-Radioactive Cell Proliferation Assay kit (MTT, Promega) according to the manufacturer's protocol. Briefly, 3-(4,5-dimethylthiazol-2-yl)-2,5-diphenyltetrazolium bromide (MTT) solution (15 μL) was added to each well. After 4 h incubation, the medium containing unreacted MTT was carefully removed. DMSO (100 μL) was added to each well to dissolve the formed formazan purple crystals, and then the absorbance at λ = 570 nm was recorded using a Powerwave HT Microplate Reader (Bio-Tek). Each concentration was replicated 6 times. Cell viability was calculated as the percent ratio of absorbance of mixtures with nanoparticles to control (cells only without NPs).

Live cell imaging. HeLa cells were plated at densities of 1× 10^5 cells/well in a 4-well glass-bottom plate (MatTek Corporation) and incubated in media (0.5 mL) at 37 ºC for 18 h. The cells were stained with Hoechst 33342 dye for 15 min. Then, the cells were washed with PBS three times to remove the dye. Phenol red free DMEM medium (0.5 mL) was added to the cells for imaging.

Appropriate amounts of free Dox or Dox-NPs were added to attain a final Dox concentration of 2.5 μg/mL. Imaging was started 10 min post-incubation for 2 hours; images were captured every 10 minutes. Cells were placed in a chamber (Live Cell Imaging) at 37 ºC with 5% CO_2 and imaged using an epifluorescence microscope with a 40x/0.95NA objective. Dox and Hoescht 33342 were excited at 405 nm and at 555 nm, respectively. In another set, HeLa cells were incubated with Dox-NPs (encapsulated Dox = 2.5 μg/mL) and free Dox for 12 hrs to examine the intracellular release of Dox from Dox-NPs; images were captured after 12 hrs of incubation with the same microscope setting.

Flow cytometry. HeLa cells were plated at densities of 5×10^5 cells/well in 6-well dishes and kept at 37 °C. After 24 h, cells were treated with Dox-NPs (48.6 μL, encapsulated Dox = 2.5 μg/mL) for either 30 min or 12 h. After, the cells were washed with DMEM and treated with trypsin. The cells were suspended in DMEM (500 μL) for flow cytometry measurements using a FACSCanto II flow cytometer (BD Biosciences) and FACSDiva software (BD Biosciences).

Multi-cellular tumor spheroids. Multi-cellular tumor spheroids (MCTS) were generated from HeLa and A549 cells in 96-well plates (BioLite, Thermo Scientific). Wells were coated with 1.5% agarose (Biotechnology Grade, BioShop), then seeded with 500-1000 cells in 150 μl of growth medium, which were left to aggregate with gravity at 37 °C and 5% CO_2. MCTS were grown for 6 to 10 days, and were monitored daily using an Inverted Invertoskop 40 C light microscope. Once MCTS formation was confirmed, they were transferred into 24-well plates coated with agarose in 2 mL of growth medium. MCTS were incubated with Dox-NPs (encapsulated Dox = 1.6 μg/mL), free Dox (1.6 μg/mL) or DPE-NPs (270 μg/mL; control) for 4 days to compare Dox penetration. Images of the spheroids were acquired using the epifluorescence microscope with 4x objective; Dox was excited at 488 nm. Quantitative analysis of the entire surface area of each spheroid was measured and normalized to their initial values at time = 0, thereby giving the fluorescence intensity relative to the first values.

Cellular uptake of Dox-NPs. HeLa cells were plated on 25 mm round coverslips (No. 1.5) at 40-50% confluency and kept at 37 ºC with 5% CO_2 using a heated chamber (Tokai Hit). Cells were pre-treated for 1 hr with (i) 100 μM Genistein (GEN) to block caveolae-mediated endocytosis, (ii) 5 μM Chlorpromazine Hydrochloride (CPZ) to block clathrin-dependent receptor-mediated endocytosis, or (iii) 100 μM Genistein and 5 μM Chlorpromazine Hydrochloride in combination to block both pathways simultaneously. Cell nuclei were stained with Hoechst 33342 dye prior to imaging. The round coverslips were then placed in a 35 mm Chamlide magnetic chamber (Quorum).

Cells were imaged for 1 hr before and after treatment with a final concentration of encapsulated Dox = 2.5 μg/mL. Live imaging was performed on CLSM using 60x/1.4NA oil immersion objective. Dox and Hoescht 33342 were excited at 405 nm and at 488 nm, respectively. The settings were kept the same for control cells and each treatment. Z-stacks of 0.5 μm were taken every 5 minutes.

Results and Discussion

Preparation of DPE and DPE-based NP colloids. A dual enzyme and oxidation-responsive polyester (DPE) containing both sulfide and ester linkages on the backbone were synthesized by a highly efficient "click" type base-catalyzed thiol-ene polyaddition reaction. The detailed synthesis and characterization are described in Supporting Information (Figure S1).

DPE is hydrophobic, and thus needs external stabilizers to form colloidally-stable NPs in aqueous solution. To prepare aqueous NPs, combined stabilizers consisting of PEG and B20 were empolyed. PEG is biocompatible and FDA-approved for clinincal use; has low cytotoxicity; provides excellent sheath effect; and prevents nonspecific protein adsorption.[45, 46] However, PEG used here has relatively high molecular weight with MW = 6,000 g/mol and thus has low ability to reduce the surface tension of water due its tendency to hydrophilicity.[47, 48] B20 has a low molecular weight stabilizer consisting of the short chains of hydrophilic PEG (MW = 800 g/mol) and a hydrophobic stearyl group.[49] The addition of B20 to the PEG stabilizing system allowed for the synthesis of a colloidally-stable DPE NP dispersion. Figure 2a shows a DLS diagram of the formed colloids in the presence of PEG/B20 stabilizers under the conditions of DPE = 0.9 mg/mL, (PEG+B20)/DPE = 1/1, and B20/PEG = 5% (by weight) on total stabilizers. The formed NPs had a diameter = 120 ± 1 nm (by intensity). TEM analysis indicates the NPs had a diameter = 116 ± 12 nm in dehydrated states.

Enzyme and oxidation-responsive disassembly. Enzyme-responsive disassembly was examined as aqueous NPs were mixed with 10 U esterase (Figure 2b). After 7 hrs of incubation with enzyme, both DLS diagram and TEM image show the size increase in NPs with multimodal distribution due to large aggregation. As control with esterase only in aqueous solution (without NPs), no significant change in size distribtion of esterase was observed over 1 day (Figure S2). Similar result showing NP size increase is reported for enzyme-degradable hypebranched polyphosphoester micelles.[50] Furthermore, the quantitative analysis using a GPC technique to show a decrease in molecular weight of copolymer by enzymatic cleavage of ester and phosphoester linkages is reported.[51] Based on

these reported results, our result showing the change in size distribution could be attributed to the destabilization of colloids upon the enzymatic cleavage of backbone ester linkages in the response to the enzymatic reaction.

Next, oxidation-responsive disassembly was followed with 1% hydrogen peroxide. Different from enzymatic reaction, both DLS and TEM images show that the NPs decreased in size with the diameter ≈59 nm after 48 hrs of incubation (Figure 2c). Similar result of decrease in NP sizes in response to hydrogen peroxide has been reported.[52] Such a change in size distribution could be due to the oxidation-response of sulfide linakges to the corresponding sulfoxide and sulfone ones, as described in reports where ^{1}H-NMR was used for the quantitiatve analysis of the oxidation of backbone thioether groups in the presence of hydrogen peroxide.[53, 54]

Preparation and colloidal stability of Dox-loaded NPs. To assess the use of DPE-NPs as tumor-targeting intracellular drug delivery nanocarriers, Dox, a clinically-used anticancer drug, was encapsulated in the NPs. A mixure consisting of an organic solution of DPE and Dox with an aqueous solution of stabilizers was placed in dialysis tubing (MWCO = 12,000 g/mol) and dialyzed against water for 6 hrs. This procedure allows for the removal of excess Dox and Et_3N, yielding colloidally-stable aqueous Dox-NPs at a concentration of 2.0 mg/mL. The capacity and efficiency of loading Dox in NPs was analyzed. The extinction coefficient of Dox in a mixture of water/THF at 1/4 v/v was determined to be 8,700 M^{-1} cm^{-1} (see Figure S3 for overlaid UV spectra of Dox and linear progression of absorbance at λ_{max} = 498 nm over various concentrations). An aliquot of aqueous Dox-NPs was dissolved in a mixture of water/THF = 1/4 v/v and their UV spectrum were recorded (Figure S4a). Using the Beer-Lambert equation with the predetermined extinction coefficient of Dox in water/THF = 1/4 v/v, the loading level of Dox was 3.6% and encapsulation efficiency was 64%. DLS analysis showed that the diameter of loaded NPs was 144 ± 1 nm, which was larger than that of the empty NPs. Further, Dox-NPs had a monomodal distribution with no evidence of aggregation (Figure S4b).

The formed Dox-NPs were evaluated for their shelf-life colloidal stability using DLS. Their diameter was unchanged with no precipitation at room temperature over 330 days (Figure S5a). Next, they were then examined for non-specific interaction of Dox-NPs with serum (plasma) proteins was examined. Serum proteins can form a “protein corona” around NPs, which results in their rapid elimination from blood circulation and is highly undesirable.[55, 56] Two of the more abundant proteins in blood were examined: BSA (35 – 52 g/L) and human IgG (8 – 16 g/L). Aliquots of Dox-

NPs were incubated with BSA (40 g/L) and IgG (8 g/L) in PBS at pH = 7.2 for 48 hrs. They were centrifuged to remove aggregates formed by undesired interactions of NPs with proteins, then the supernatants were analyzed using BCA assays to quantify the interaction of NPs with proteins. As Figure S5b shows, both BSA and IgG proteins in the supernatants were determined to be >90%. This result suggests that these common serum proteins do not cause large aggregation, and thus the NPs should have excellent colloidal stability.

Enhanced release of encapsulated Dox and model drug. The Dox-NPs were examined for their ability to release in response to enzyme and oxidation. First, enzyme-responsive enhanced release of Dox from Dox-NPs was examined using UV/Vis spectroscopy. An aliquot of Dox-NPs was placed in dialysis tubing (MWCO = 12 kDa) and submerged in PBS containing 10 U or 20 U esterase. Similar concentrations of esterase were examined for esterase-responsive block copolymer micelles[57] and peptide amphiphile-based nanofibers.[58] Aliquots of outer water were taken periodically to record the UV/Vis spectra (Figure S6). Then, the absorbance at λ_{max} = 498 nm was followed to investigate %Dox release. As seen in Figure 3, <20% Dox was released from Dox-NPs in the absence of esterase. In the presence of esterase, the backbone ester linkages should be targeted, causing destabilization (or disintegration) of Dox-NPs to enhance the release of Dox. The released Dox molecules should diffuse through the dialysis tubing into outer water and thus the absorbance of Dox in outer water increases. Compared with other supramolecular nanostructures,[58] where the change in esterase concentration does not have any effect, Dox release occurred in the presence of 10 U esterase, and was faster in the presence of 20 U esterase. For example, %Dox reached to as high as 85% with 20 U esterase, compared to 60% with 10 U esterase.

The oxidation-responsive release of Dox from Dox-NPs in response to hydrogen peroxide was determined. However, due to the instability of Dox in hydrogen peroxide (1% v/v), the experimental approach had to be modified. As seen in our control experiment where Dox was incubated with 1% hydrogen peroxide, the absorbance of Dox decreased gradually over the incubation time (Figure S7).

A hydrophobic model for anti-cancer drugs is Nile Red (NR), which is stable for at least 170 h in hydrogen peroxide (5% v/v).[52] Thus, NR-loaded NPs were used as an alternative approach to monitor oxidation-responsive release in the presence of hydrogen peroxide using fluorsecence spectroscopy. This method can determine changes in the fluorescence intensity of NR in different conditions, which would change due to its low solubility in water. NR fluorescence is intense when encapsulsted in hydrophobic cores. However, the intensity significantly decreases when NR molecules are released and exposed to water as a consequence of the destabilization of NR-loaded NPs.[59, 60]

Here, the solvent evaporation method was used to prepare aqueous NR-loaded NPs (NR-NPs) with a diameter = 153 nm (Figure S8). Aliquots were incubated with 1% and 5% hydrogen peroxide and their emission spectra were followed over time (Figure S9). In the absence of hydrogen peroxide, the fluorescence intensity of NR-NPs at 620 nm remained unchanged, suggesting that NR was not released or photobleached. In the presence of hydrogen peroxide, the flourescence intensity decreased with kinetics that is correlated with changes in the concentration of hydrogen peroxide (Figure 4a). For example, the intensity rapidly decreased to less than 10% within 8 hrs with 5% hydrogen peroxide, while it gradually decreased to similar level in 45 hrs. Such a hydrogen peroxide concentration-dependent release of NR is reported at 0.15-3.3% hydrogen peroxide for self-assembled micelles based on a diblock copolymer consisting of poly(propylene sulfide) and poly(N,N-dimethylacrylamide) blocks.[52] In addition, the change in hydrophilic/hydrophobic balance upon oxidation is also reported at 0.3-1% hydrogen peroxide for polysulfides.[42, 54, 61]

Interestingly, there was an increase in intensity in 1% hydrogen peroxide. This unusual phenomenon could be attributed to self-quenching of NR molecules confined in small-sized NR-loaded NPs. Upon destabilization of NR-loaded NPs in response to hydrogen peroxide, NP cores could swell, resulting in a decrease in self-quenching of NR molecules. After longer incubation, the fluorescence intensity decreased, likely due to further destabilization of NPs.[62, 63] In another analysis, the emission wavelength of maximum fluorescence intensity ($\lambda_{em,max}$) was monitored. As seen in Figure 4b, the $\lambda_{em,max}$ increased from 620 nm to 640 nm (max) over the incubation time. This increase in wavelength is similar to the decrease in intensity. Given that the $\lambda_{em,max}$ of NR is red-shifted when the polarity of the medium increases. This increase could arise due to the release of NR molecules from NPs upon oxidative degradation.

Together, these results show the enhanced release of encapsulated drugs (Dox and NR) from DPE-NPs in response to both enzymatic activity and oxidation. Nevertheless, further efforts could be made to optimize the design of DPE-based NPs targeting the synergistic release profile upon dual stimuli-responsive degradation at biologically-relevant concentrations of esterase and ROS.

Activity and intracellular uptake in HeLa cells. The cytotoxicity of DPE-NPs was evaluated on HeLa cervical cancer cells. Dox-loaded NPs were compared with empty NPs using a MTT colorimetric assay. As seen in Figure 5a, HeLa cell viability was >85% in the presence of empty NPs up to 500 μg/mL, suggesting non-toxicity of empty NPs to HeLa cells. When incubated with NPs

loaded with Dox = 1.7 μg/mL (equivalent to 100 μg/mL of Dox-NPs), the viability of HeLa cells decreased to 44% (Figure 5b). The decreased viability suggests that the proliferation of HeLa cells was inhibited by the Dox-NPs. When HeLa cells were treated with the same concentration of free Dox, cell viability significantly decreased to <10%, suggesting that free Dox more effectively blocks HeLa cell proliferation over 48 hrs, or two doubling times, compared with Dox-NPs.

Next, the intracellular localization of Dox-NPs was explored using fluorescence microscopy (Supplemental movie M1 and M2). Figure 6a shows fluorescence images of HeLa cells 10 min (t = 0) and 2 hrs after incubation with free Dox or Dox-NPs. The nuclei were stained with Hoechst 33342, shown in blue, and Dox fluorescence is shown in red. Dox fluorescence increased with time in cells treated with free Dox or Dox-NPs. However, Dox was seen in the nuclei in cells treated with free Dox, while Dox was in the perinuclear region rich in endomembrane networks in cells treated with Dox-NPs. Therefore, the NPs likely enter cells via endocytosis and traffic to the endomembrane system, where their release may be more highly controlled vs. free Dox molecules. Followed by the accumulation in the perinuclear region, Dox accumulated in the nuclei post 12 hrs of incubation. This is ascribed to the intracellular release of Dox from Dox-NPs (Figure S10). The intracellular accumulation of Dox was also monitored using flow cytometry. HeLa cells were analysed using flow cytometry after 30 min and 12 hrs of incubation with free Dox or Dox-NPs. As shown in Figure 6b, the histogram for free Dox was shifted to higher fluorescence intensity, compared with Dox-NPs after 30 min of incubation. After 12 hrs, the histogram for Dox-NPs shifted to higher fluorescence intensity compared with free Dox (Figure 6c). These changes are more obvious in Figure 6b-e. While there was only a slight increase in intensity for free Dox between 30 min and 12 h of incubation, there was a significant increase in intensity for Dox-NPs. This result suggests that the internalization of free Dox occurs very rapidly, but reaches a threshold with no further internalization. In contrast, the internalization of Dox-NPs gradually increases over time with a greater threshold.

Uptake by cells in multicellular tumor spheroids. Multicellular tumor spheroids (hereafter referred to as spheroids) grown from cultured cells *in vitro* have properties that mimic solid tumors *in vivo*, and thus serve as a model to predict the ability of drug-loaded NPs to penetrate tumors.[64] Here, HeLa cells were induced to form spheroids and incubated with Dox-NPs or free Dox at 1.6 μg/mL, or empty DPE NPs as a control for 4 days. The bright field and fluorescence images of HeLa spheroids in Figure 7a show the difference in fluorescence intensity between Dox-NPs and free Dox. Further quantitative analysis in Figure 7b-c indicates that Dox-NPs show a sharp increase in fluorescence

within 6 hrs; and upon further incubation, the signal steadily increased. After 4 days of incubation, spheroids with Dox-NPs had intensities that were five times greater than spheroids with free Dox. These results suggest that Dox-NPs are superior in their ability to ~~penetrate~~ accumulate in HeLa spheroids compared with free Dox. Thus, the controlled uptake and increased threshold of Dox-NPs could contribute to an overall increased efficacy of uptake at the multicellular level. To determine if Dox-NPs can also efficiently penetrate spheroids made from other cell types, a similar experiment was performed using spheroids made from A549 lung cancer cells (Figure S11). The uptake of Dox-NPs in A549 spheroids was greater than free Dox, suggesting that the NPs enhance uptake with multiple cancers. Such enhanced cellular uptake could be the result of the combination of nanoparticle characteristics such as size, morphology, and surface charge.

Endocytic uptake of Dox-NPs in HeLa cells. Polymer-based or inorganic NPs can be internalized through several pathways such as clathrin- or caveolae-mediated endocytosis, and macropinocytosis.[65-68] As shown in Figure 7, Dox-NPs were visualized in the endomembrane system, supporting that they were taken into cells via one of these mechanisms. To gain insight into the mechanism of entry for the DPE NPs, HeLa cells were incubated with Dox-NPs after being treated without (control) or with chlorpromazine, genistein or a combination of both inhibitors. It has been reported that chlorpromazine inhibits clathrin-mediated endocytosis,[69] while genistein inhibits caveolae-mediated endocytosis.[70] Thus, blocking the pathway that mediates the uptake of Dox-NPs should result in no fluorescence signal inside cells. Figure 8a shows the fluorescence images of HeLa cells treated with Dox-NPs for 1 hr. The red color represents the fluorescence Dox signal, while blue shows the nuclei. Figure 8b shows the quantitative analysis of Dox fluorescence intensity for each treatment normalized to maximum intensity for control (no inhibitors) over 1 hr. While control cells reached a maximum of 100% of normalized intensity after 1 hr, this signal was reduced to 50% after treatment with chlorpromazine and remained at 0% after genistein treatment, or when treated with both inhibitors. These results suggest that caveolae-mediated endocytosis is the dominant pathway for the internalization of Dox-NPs into HeLa cells. Furthermore, the results implicate the reason why Dox-NPs exhibit relatively less cytotoxicity, compared with free Dox, although they had greater cellular uptake based on flow cytometry results. Clathrin-mediated endocytosis and macropinocytosis carry NPs to lysosomes, which are acidic pH (4.5-5.5) and have degradative enzymes. Under these conditions, the NPs could be degraded, resulting in enhanced release of encapsulated Dox. On the other hand, caveolae-mediated endocytosis carries caveolar vesicles to caveosomes; thus the release of Dox is delayed through this endocytosis mechanism.[66, 71] However, the controlled release of Dox

from NPs could be more beneficial over longer periods time in the context of tumors *in vivo*, as the capacity for their uptake is higher, this could result in a more tightly controlled release of Dox vs. rapid accumulation of free Dox at lower levels.

Conclusion

Dual enzyme/oxidation-responsive DPEs with ester and sulfide linkages on their backbones was synthesized by a thiol-ene polyaddition reaction. DPEs were fabricated into aqueous DPE-NP colloids with a diameter = 120 nm, which were non-toxic to HeLa cells up to 750 μg/mL. They were stable and exhibited prolonged colloidal stability when kept for long periods of time on the shelf, or in the presence of serum proteins to mimic physiological conditions. The NPs disassembled successfully in the presence of esterase and hydrogen peroxide, upon cleavages of the ester linkages and oxidation of the sulfide linkages, respectively, as confirmed by DLS analysis. Such dual stimuli-responsive degradation enabled the enhanced and controlled release of encapsulated Dox (clinical anticancer drug) and NR (fluorescent dye as a model hydrophobic drug) from NPs. Dox-NPs inhibited the proliferation of HeLa cells and excitingly, they were internalized with higher thresholds compared to free Dox, confirmed by the results from HeLa or A549 cells grown in 2D or 3D spheroids. Further, Dox-NPs appeared to enter cells predominantly by caveolae-mediated endocytosis, which would protect them from degradation in the lysosomes and permit more controlled release. These results suggest that aqueous DPE-NPs hold a potential as an efficient intracellular nanocarrier that can deliver anti-cancer therapeutics to inhibit solid tumors.

Acknowledgements

This work is supported from Natural Science and Engineering Research Council (NSERC) in Canada through Discovery Grants for JKO and AP as well as Canada Research Chair (CRC) Award for JKO. JKO is entitled Tier II CRC in Nanobioscience (renewed in 2016). Authors thank tremendous helps from Dr. Chris Law (Center of Concordia Microscopy) for his fluorescence-based cellular imaging experiments as well as Dr. Gael Dulude (Institute for Research in Immunology and Cancer at the University of Montreal) for flow cytometry experiments.

References

[1] P.G. Corrie, Cytotoxic chemotherapy: clinical aspects, Medicine, 36 (2008) 24-28.

[2] D.B. Reuben and V. Mor, Nausea and vomiting in terminal cancer patients, Arch. Intern. Med., 146 (1986) 2021-2023.

[3] T. Sun, Y.S. Zhang, B. Pang, D.C. Hyun, M. Yang and Y. Xia, Engineered nanoparticles for drug delivery in cancer therapy, Angew. Chem. Int. Ed., 53 (2014) 12320-12364.

[4] Y. Matsumura and K. Kataoka, Preclinical and clinical studies of anticancer agent-incorporating polymer micelles, Cancer Sci., 100 (2009) 572-579.

[5] A.S. Mikhail and C. Allen, Block copolymer micelles for delivery of cancer therapy: Transport at the whole body, tissue and cellular levels, J. Controlled Release, 138 (2009) 214-223.

[6] Y.H. Bae and K. Park, Targeted drug delivery to tumors: Myths, reality and possibility, J. Controlled Release, 153 (2011) 198-205.

[7] F. Danhier, O. Feron and V. Préat, To exploit the tumor microenvironment: Passive and active tumor targeting of nanocarriers for anti-cancer drug delivery, J. Controlled Release, 148 (2010) 135-146.

[8] A.E.v.d. Ende, E.J. Kravitz and E. Harth, Approach to formation of multifunctional polyester particles in controlled nanoscopic dimensions, J. Am. Chem. Soc., 130 (2008) 8706-8713.

[9] G.B. Jacobson, R. Shinde, C.H. Contag and R.N. Zare, Sustained release of drugs dispersed in polymer nanoparticles, Angew. Chem. Int. Ed., 47 (2008) 7880-7882.

[10] D. Brambilla, J. Nicolas, B. Le Droumaguet, K. Andrieux, V. Marsaud, P.-O. Couraud and P. Couvreur, Design of fluorescently tagged poly(alkyl cyanoacrylate) nanoparticles for human brain endothelial cell imaging, Chem. Commun., 46 (2010) 2602-2604.

[11] S. Taurin, H. Nehoff and K. Greish, Anticancer nanomedicine and tumor vascular permeability; Where is the missing link?, J. Controlled Release, 164 (2012) 265-275.

[12] L. Zhang, Y. Li and J.C. Yu, Chemical modification of inorganic nanostructures for targeted and controlled drug delivery in cancer treatment, J. Mater. Chem. B, 2 (2014) 452-470.

[13] J.W. Nichols and Y.H. Bae, Odyssey of a cancer nanoparticle: From injection site to site of action, Nano Today, 7 (2012) 606-618.

[14] C.J.F. Rijcken, O. Soga, W.E. Hennink and C.F. van Nostrum, Triggered destabilization of polymeric micelles and vesicles by changing polymers polarity: An attractive tool for drug delivery, J. Controlled Release, 120 (2007) 131-148.

[15] Q. Zhang, N.R. Ko and J.K. Oh, Recent advances in stimuli-responsive degradable block copolymer micelles: synthesis and controlled drug delivery applications, Chem. Commun., 48 (2012) 7542-7552.

[16] H. Wei, R.-X. Zhuo and X.-Z. Zhang, Design and development of polymeric micelles with cleavable links for intracellular drug delivery, Prog. Polym. Sci., 38 (2013) 503-535.

[17] S. Mura, J. Nicolas and P. Couvreur, Stimuli-responsive nanocarriers for drug delivery, Nat. Mater., 12 (2013) 991-1003.

[18] C. Alvarez-Lorenzo and A. Concheiro, Smart drug delivery systems: from fundamentals to the clinic, Chem. Commun., 50 (2014) 7743-7765.

[19] R.V. Ulijn, Enzyme-responsive materials: a new class of smart biomaterials, J. Mater. Chem., 16 (2006) 2217-2225.

[20] M.H. Lee, Z. Yang, C.W. Lim, Y.H. Lee, D. Sun, C. Kang and J.S. Kim, Disulfide-Cleavage-Triggered Chemosensors and Their Biological Applications, Chem. Rev., 113 (2013) 5071-5109.

[21] B.S. Bolu, B. Golba, N. Boke, A. Sanyal and R. Sanyal, Designing Dendron-Polymer Conjugate Based Targeted Drug Delivery Platforms with a "Mix-and-Match" Modularity, Bioconjugate Chemistry, 28 (2017) 2962-2975.

[22] C. Deng, Y. Jiang, R. Cheng, F. Meng and Z. Zhong, Biodegradable polymeric micelles for targeted and controlled anticancer drug delivery: Promises, progress and prospects, Nano Today, 7 (2012) 467-480.

[23] M. Huo, J. Yuan, L. Tao and Y. Wei, Redox-responsive polymers for drug delivery: from molecular design to applications, Polym. Chem., 5 (2014) 1519-1528.

[24] S. Binauld and M.H. Stenzel, Acid-degradable polymers for drug delivery: a decade of innovation, Chem. Commun., 49 (2013) 2082-2102.

[25] I.R. Fernando, D.P. Ferris, M. Frasconi, D. Malin, E. Strekalova, M.D. Yilmaz, M.W. Ambrogio, M.M. Algaradah, M.P. Hong, X. Chen, M.S. Nassar, Y.Y. Botros, V.L. Cryns and J.F. Stoddart, Esterase- and pH-responsive poly(β-amino ester)-capped mesoporous silica nanoparticles for drug delivery, Nanoscale, 7 (2015) 7178-7183.

[26] L.A. Needham, A.H. Davidson, L.J. Bawden, A. Belfield, E.A. Bone, D.H. Brotherton, S. Bryant, M.H. Charlton, V.L. Clark and S.J. Davies, Drug targeting to monocytes and macrophages using esterase-sensitive chemical motifs, J. Pharmacol. Exp. Ther., 339 (2011) 132-142.

[27] L. Zhu, P. Kate and V.P. Torchilin, Matrix Metalloprotease 2-Responsive Multifunctional Liposomal Nanocarrier for Enhanced Tumor Targeting, ACS Nano, 6 (2012) 3491-3498.

[28] R. Dorresteijn, N. Billecke, M. Schwendy, S. Puetz, M. Bonn, S.H. Parekh, M. Klapper and K. Muellen, Polylactide-block-polypeptide-block-polylactide copolymer nanoparticles with tunable cleavage and controlled drug release, Adv. Funct. Mater., 24 (2014) 4026-4033.

[29] L. Gao, B. Zheng, W. Chen and C.A. Schalley, Enzyme-responsive pillar[5]arene-based polymer-substituted amphiphiles: synthesis, self-assembly in water, and application in controlled drug release, Chem. Commun., 51 (2015) 14901-14904.

[30] N. Li, H. Cai, L. Jiang, J. Hu, A. Bains, J. Hu, Q. Gong, K. Luo and Z. Gu, Enzyme-Sensitive and Amphiphilic PEGylated Dendrimer-Paclitaxel Prodrug-Based Nanoparticles for Enhanced Stability and Anticancer Efficacy, ACS Appl. Mater. Interfaces, 9 (2017) 6865-6877.

[31] W. Yin, J. Li, W. Ke, Z. Zha and Z. Ge, Integrated Nanoparticles To Synergistically Elevate Tumor Oxidative Stress and Suppress Antioxidative Capability for Amplified Oxidation Therapy, ACS Appl. Mater. Interfaces, 9 (2017) 29538-29546.

[32] S.G. Levesque and M.S. Shoichet, Synthesis of Enzyme-Degradable, Peptide-Cross-Linked Dextran Hydrogels, Bioconjugate Chemistry, 18 (2007) 874-885.

[33] M. Segal, R. Avinery, M. Buzhor, R. Shaharabani, A.J. Harnoy, E. Tirosh, R. Beck and R.J. Amir, Molecular Precision and Enzymatic Degradation: From Readily to Undegradable Polymeric Micelles by Minor Structural Changes, J. Am. Chem. Soc., 139 (2017) 803-810.

[34] I. Rosenbaum, A.J. Harnoy, E. Tirosh, M. Buzhor, M. Segal, L. Frid, R. Shaharabani, R. Avinery, R. Beck and R.J. Amir, Encapsulation and Covalent Binding of Molecular Payload in Enzymatically Activated Micellar Nanocarriers, J. Am. Chem. Soc., 137 (2015) 2276-2284.

[35] J. Guo, J. Zhuang, F. Wang, K.R. Raghupathi and S. Thayumanavan, Protein AND Enzyme Gated Supramolecular Disassembly, J. Am. Chem. Soc., 136 (2014) 2220-2223.

[36] M.-H. Xiong, Y. Bao, X.-J. Du, Z.-B. Tan, Q. Jiang, H.-X. Wang, Y.-H. Zhu and J. Wang, Differential Anticancer Drug Delivery with a Nanogel Sensitive to Bacteria-Accumulated Tumor Artificial Environment, ACS Nano, 7 (2013) 10636-10645.

[37] H. Sun, R. Cheng, C. Deng, F. Meng, A.A. Dias, M. Hendriks, J. Feijen and Z. Zhong, Enzymatically and Reductively Degradable α-Amino Acid-Based Poly(ester amide)s: Synthesis, Cell Compatibility, and Intracellular Anticancer Drug Delivery, Biomacromolecules, 16 (2015) 597-605.

[38] D. Trachootham, J. Alexandre and P. Huang, Targeting cancer cells by ROS-mediated mechanisms: a radical therapeutic approach?, Nat. Rev. Drug Dis., 8 (2009) 579-591.

[39] S. Kawanishi, Y. Hiraku, S. Pinlaor and N. Ma, Oxidative and nitrative DNA damage in animals and patients with inflammatory diseases in relation to inflammation-related carcinogenesis, Biological Chem., 387 (2006).

[40] B.L. Allen, J.D. Johnson and J.P. Walker, Encapsulation and Enzyme-Mediated Release of Molecular Cargo in Polysulfide Nanoparticles, ACS Nano, 5 (2011) 5263-5272.

[41] K. Kim, C.-S. Lee and K. Na, Light-controlled reactive oxygen species (ROS)-producible polymeric micelles with simultaneous drug-release triggering and endo/lysosomal escape, Chem. Commun., 52 (2016) 2839-2842.

[42] F.H. Sobotta, F. Hausig, D.O. Harz, S. Hoeppener, U.S. Schubert and J.C. Brendel, Oxidation-responsive micelles by a one-pot polymerization-induced self-assembly approach, Polym. Chem., 9 (2018) 1593-1602.

[43] C. de Gracia Lux, S. Joshi-Barr, T. Nguyen, E. Mahmoud, E. Schopf, N. Fomina and A. Almutairi, Biocompatible Polymeric Nanoparticles Degrade and Release Cargo in Response to Biologically Relevant Levels of Hydrogen Peroxide, J. Am. Chem. Soc., 134 (2012) 15758-15764.

[44] M. Zhang, C.-C. Song, F.-S. Du and Z.-C. Li, Supersensitive Oxidation-Responsive Biodegradable PEG Hydrogels for Glucose-Triggered Insulin Delivery, ACS Appl. Mater. Interfaces, 9 (2017) 25905-25914.

[45] L. Brannon-Peppas, Poly(ethylene glycol): Chemistry and biological applications, edited by J. M. Harris and S. Zalipsky, J. Control. Release, 66 (2000) 321.

[46] K. Knop, R. Hoogenboom, D. Fischer and U.S. Schubert, Poly(ethylene glycol) in Drug Delivery: Pros and Cons as Well as Potential Alternatives, Angew. Chem., Int. Ed., 49 (2010) 6288-6308.

[47] M.W. Kim, Surface activity and property of polyethyleneoxide (PEO) in water, Colloids Surf., A, 128 (1997) 145-154.

[48] B.H. Cao and M.W. Kim, Molecular weight dependence of the surface tension of aqueous poly(ethylene oxide) solutions, Faraday Discuss., 98 (1995) 245-252.

[49] A. Bera, K. Ojha and A. Mandal, Synergistic Effect of Mixed Surfactant Systems on Foam Behavior and Surface Tension, J. Surf. Deter., 16 (2013) 621-630.

[50] M. Yao, Y. Ma, H. Liu, M.I. Khan, S. Shen, S. Li, Y. Zhao, Y. Liu, G. Zhang, X. Li, F. Zhong, W. Jiang and Y. Wang, Enzyme degradable hyperbranched polyphosphoester micellar nanomedicines for NIR imaging-guided chemo-photothermal therapy of drug-resistant cancers, Biomacromolecules, 19 (2018) 1130-1141.

[51] W. Wang, J. Ding, C. Xiao, Z. Tang, D. Li, J. Chen, X. Zhuang and X. Chen, Synthesis of Amphiphilic Alternating Polyesters with Oligo(ethylene glycol) Side Chains and Potential Use for Sustained Release Drug Delivery, Biomacromolecules, 12 (2011) 2466-2474.

[52] M.K. Gupta, T.A. Meyer, C.E. Nelson and C.L. Duvall, Poly(PS-b-DMA) micelles for reactive oxygen species triggered drug release, J. Controlled Release, 162 (2012) 591-598.

[53] J.M. Sarapas and G.N. Tew, Poly(ether-thioethers) by Thiol-Ene Click and Their Oxidized Analogues as Lithium Polymer Electrolytes, Macromolecules 49 (2016) 1154-1162.

[54] B. Yan, Y. Zhang, C. Wei and Y. Xu, Facile synthesis of ROS-responsive biodegradable main chain poly(carbonate-thioether) copolymers, Polym. Chem., 9 (2018) 904-911.

[55] Z. Gao, T. Ma, E. Zhao, D. Docter, W. Yang, R.H. Stauber and M. Gao, Small is Smarter: Nano MRI Contrast Agents - Advantages and Recent Achievements, Small, 12 (2016) 556-576.

[56] C.D. Walkey, J.B. Olsen, H. Guo, A. Emili and W.C.W. Chan, Nanoparticle Size and Surface Chemistry Determine Serum Protein Adsorption and Macrophage Uptake, J. Am. Chem. Soc., 134 (2012) 2139-2147.

[57] S. Kashyap, N. Singh, B. Surnar and M. Jayakannan, Enzyme and Thermal Dual Responsive Amphiphilic Polymer Core–Shell Nanoparticle for Doxorubicin Delivery to Cancer Cells, Biomacromolecules, 17 (2015) 384-398.

[58] M. Conda-Sheridan, S.S. Lee, A.T. Preslar and S.I. Stupp, Esterase-activated release of naproxen from supramolecular nanofibres, Chem. Commun., 50 (2014) 13757-13760.

[59] S. Aleksanian, B. Khorsand, R. Schmidt and J.K. Oh, Rapidly thiol-responsive degradable block copolymer nanocarriers with facile bioconjugation, Polym. Chem., 3 (2012) 2138-2147.

[60] N. Chan, B. Khorsand, S. Aleksanian and J.K. Oh, A dual location stimuli-responsive degradation strategy of block copolymer nanocarriers for accelerated release, Chem. Commun., 49 (2013) 7534-7536.

[61] J. Herzberger, K. Fischer, D. Leibig, M. Bros, R. Thiermann and H. Frey, Oxidation-responsive and “clickable” poly (ethylene glycol) via copolymerization of 2-(methylthio) ethyl glycidyl ether, J. Am. Chem. Soc., 138 (2016) 9212-9223.

[62] I.N. Kurniasih, H. Liang, P.C. Mohr, G. Khot, J.P. Rabe and A. Mohr, Nile Red Dye in Aqueous Surfactant and Micellar Solution, Langmuir, 31 (2015) 2639-2648.

[63] J.A. Bohnert, B. Karamian and H. Nikaido, Optimized Nile Red Efflux Assay of AcrAB-TolC Multidrug Efflux System Shows Competition between Substrates, Antimicrob. Agents Chemother., 54 (2010) 3770-3775.

[64] Y.T. Phung, D. Barbone, V.C. Broaddus and M. Ho, Rapid generation of in vitro multicellular spheroids for the study of monoclonal antibody therapy, J. Cancer, 2 (2011) 507.

[65] T.-G. Iversen, T. Skotland and K. Sandvig, Endocytosis and intracellular transport of nanparticles: present knowledge and need for future studies, Nano Today, 6 (2011) 176-185.

[66] B. Yameen, W.I. Choi, C. Vilos, A. Swami, J. Shi and O.C. Farokhzad, Insight into nanoparticle cellular uptake and intracellular targeting, J. Controlled Release, 190 (2014) 485-499.

[67] S.-J. Seo, M. Chen, H. Wang, M.S. Kang, K.W. Leong and H.-W. Kim, Extra- and intra-cellular fate of nanocarriers under dynamic interactions with biology, Nano Today, 14 (2017) 84-99.

[68] J. Zhao and M.H. Stenzel, Entry of nanoparticles into cells: the importance of nanoparticle properties, Polym. Chem., 9 (2018) 259-272.

[69] L.H. Wang, K.G. Rothberg and R.G.W. Anderson, Mis-assembly of clathrin lattices on endosomes reveals a regulatory switch for coated pit formation, J. Cell Biol., 123 (1993) 1107-1118.

[70] R.G. Parton, B. Joggerst and K. Simons, Regulated internalization of caveolae, J. Cell Biol., 127 (1994) 1199-1216.

[71] G. Sahay, D.Y. Alakhova and A.V. Kabanov, Endocytosis of nanomedicines, J. Controlled Release, 145 (2010) 182-195.

Figure and Scheme captions

Figure 1. Schematic illustration of intracellular drug delivery of DPE-based core/shell NPs loaded with Dox.

Figure 2. DLS diagrams and TEM images (inset) of aqueous DPE NP colloids with an aid of mixed PEG/B20 stabilizers in the absence (a) and presence of 10 U esterase (b), and 1 % hydrogen peroxide (c) at 0.1 mg/mL and pH = 7.2.

Figure 3. Release profile in short-term (a) and long-term (b) time scale of Dox from Dox-NPs in the absence and presence of 10 U and 20 U esterase at pH = 7.2. Each sample was measured three times.

Figure 4. Normalized fluorescence (FL) intensity (a) and maximum wavelength of FL intensity (b) of NR at λ_{em} = 620 nm in the mixture of aqueous NR-loaded NPs incubated with hydrogen peroxide of 1% and 5%. Each sample was measured three times.

Figure 5. Viability of HeLa cells incubated with different amounts of empty NPs (a) and Dox-NPs, compared with free Dox, (b) for 48 hrs determined by an MTT assay. Data are presented as the average ± standard deviation (n = 6).

Figure 6. Time-lapse fluorescence microscopy images of HeLa cells incubated with Dox-NPs (encapsulated Dox = 1.6 μg/mL), compared with free Dox (2.5 μg/mL), for 2 hrs (a) as well as their histograms from flow cytometry after 30 min (b) and 12 hrs (c) of incubation and their comparison of free Dox-NPs (d) and Dox (e) over incubation time. Note that the images in red color (Dox) were processed differently for free Dox and Dox-NPs due to low signal from free Dox and the high signal from Dox-NPs. For all experiments, the amount of Dox-NPs was designed to have the encapsulated Dox whose concentration was kept to be 2.5 μg/mL. (Scale bar = 30 μm).

Figure 7. Florescence microscope images of HeLa spheroids incubated for 4 days with Dox NPs (encapsulated Dox = 1.6 μg/mL), free Dox (1.6 μg/mL), and empty DPE-NPs (270 μg/mL) as a control (a). Quantitative analysis of florescence intensity of the spheroids after short term (24 hrs) (b) and long term (4 days) treatments (c). Each value was normalized by their initial value. *Note that the images

were processed differently for free Dox and Dox-NPs due to low signal from free Dox and high signal from Dox-NPs. (n = 3, scale bar = 200 μm).

Figure 8. FL images of single cell incubated with Dox-NPs in the absence (control) and presence of chlorpromazine (CPZ, inhibiting clathrin-mediated endocytosis), or genistein (GEN, inhibiting caveolae-mediated endocytosis), or both inhibitors (a) and quantitative analysis of FL intensity of Dox in the perinuclear region normalized with maximum FL intensity of control system (no inhibitors) over 1 hr (b) (scale bar = 10 μm).

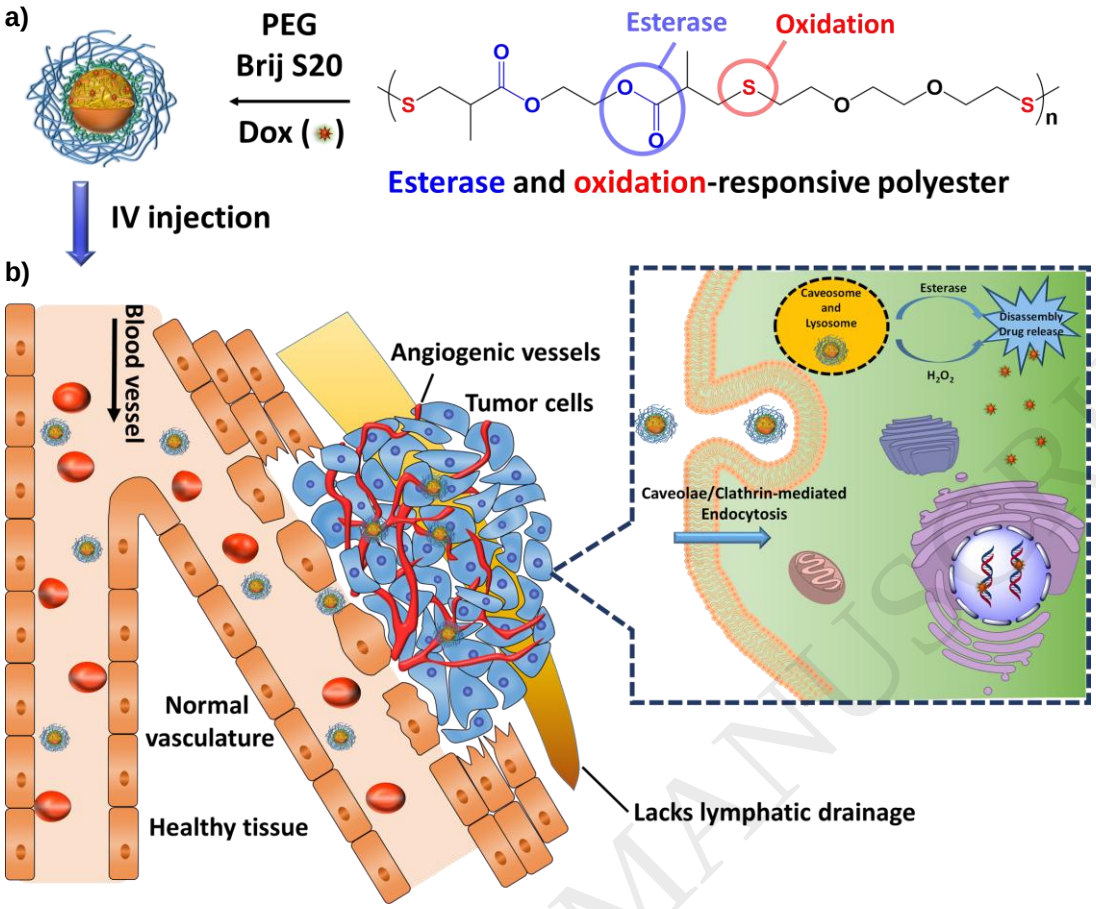

Figure 1. Schematic illustration of intracellular drug delivery of DPE-based core/shell NPs loaded with Dox.

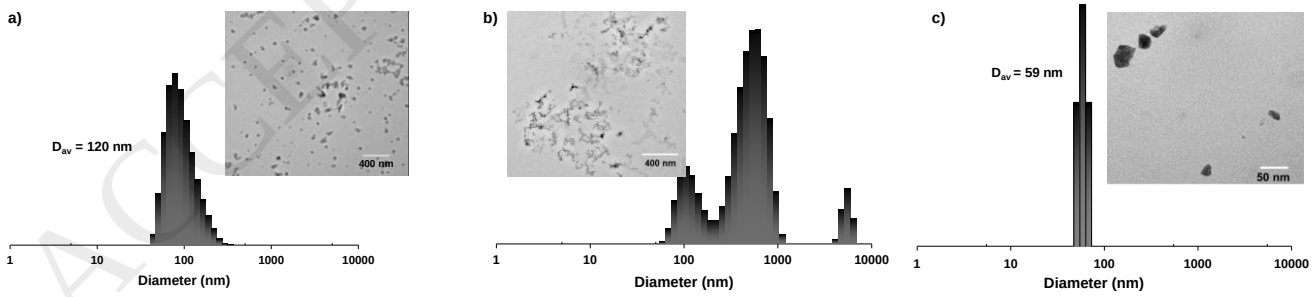

Figure 2. DLS diagrams and TEM images (inset) of aqueous DPE NP colloids with an aid of mixed PEG/B20 stabilizers in the absence (a) and presence of 10 U esterase (b), and 1 % hydrogen peroxide (c) at 0.1 mg/mL and pH = 7.2.

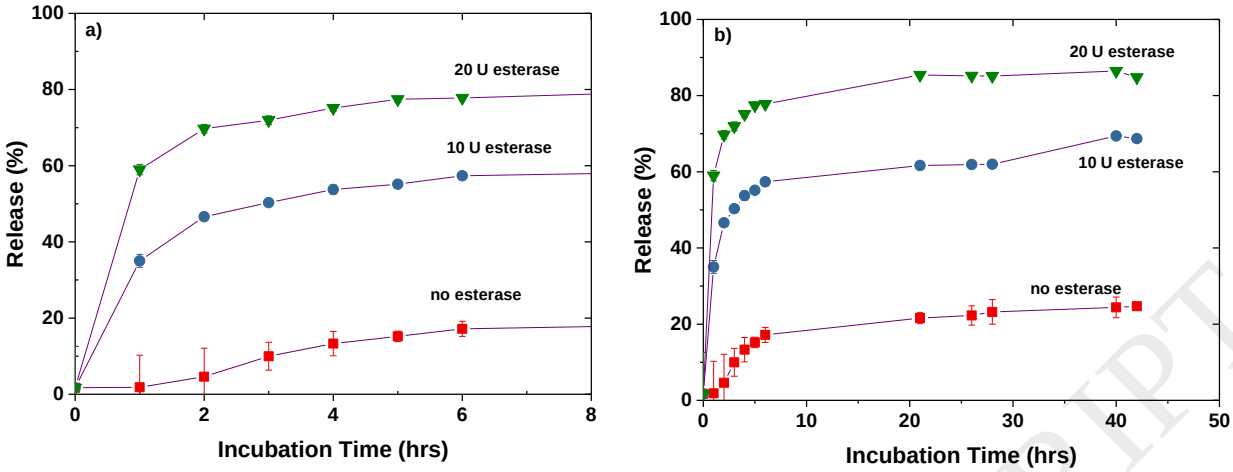

Figure 3. Release profile in short-term (a) and long-term (b) time scale of Dox from Dox-NPs in the absence and presence of 10 U and 20 U esterase at pH = 7.2. Each sample was measured three times.

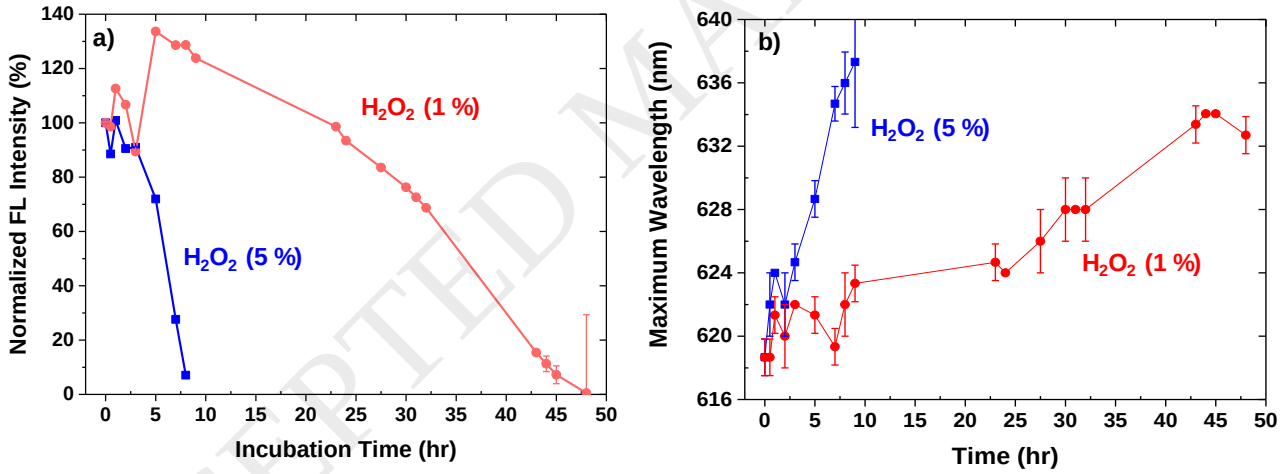

Figure 4. Normalized fluorescence (FL) intensity (a) and maximum wavelength of FL intensity (b) of NR at λ_{em} = 620 nm in the mixture of aqueous NR-loaded NPs incubated with hydrogen peroxide of 1% and 5%. Each sample was measured three times.

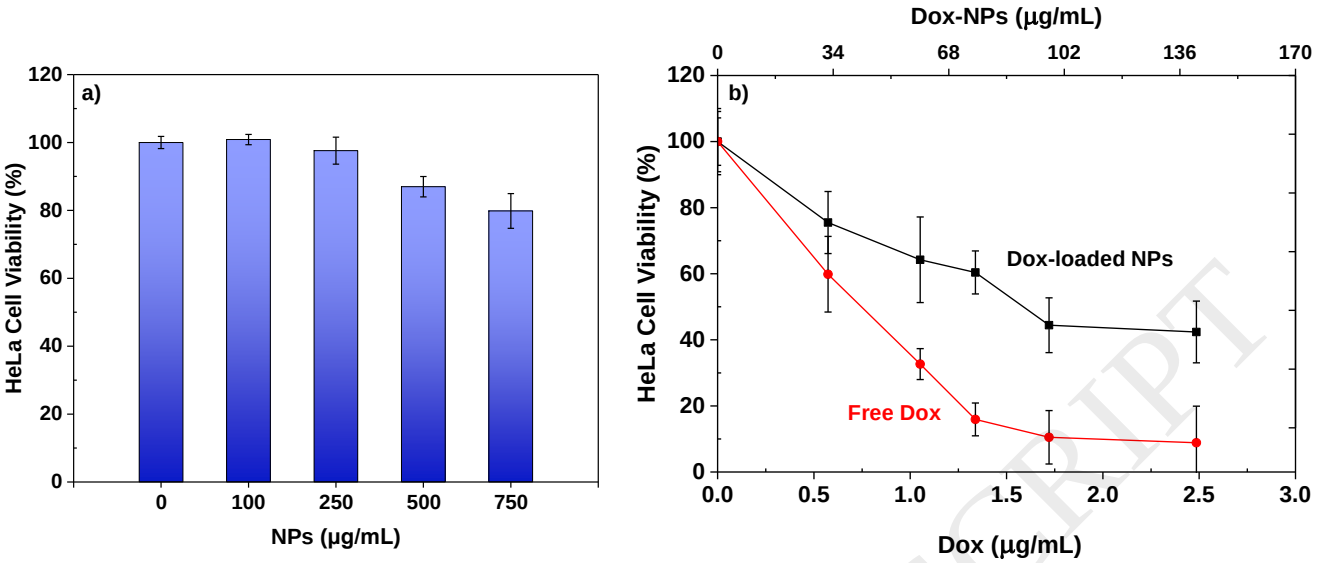

Figure 5. Viability of HeLa cells incubated with different amounts of empty NPs (a) and Dox-NPs, compared with free Dox, (b) for 48 hrs determined by an MTT assay. Data are presented as the average ± standard deviation (n = 6).

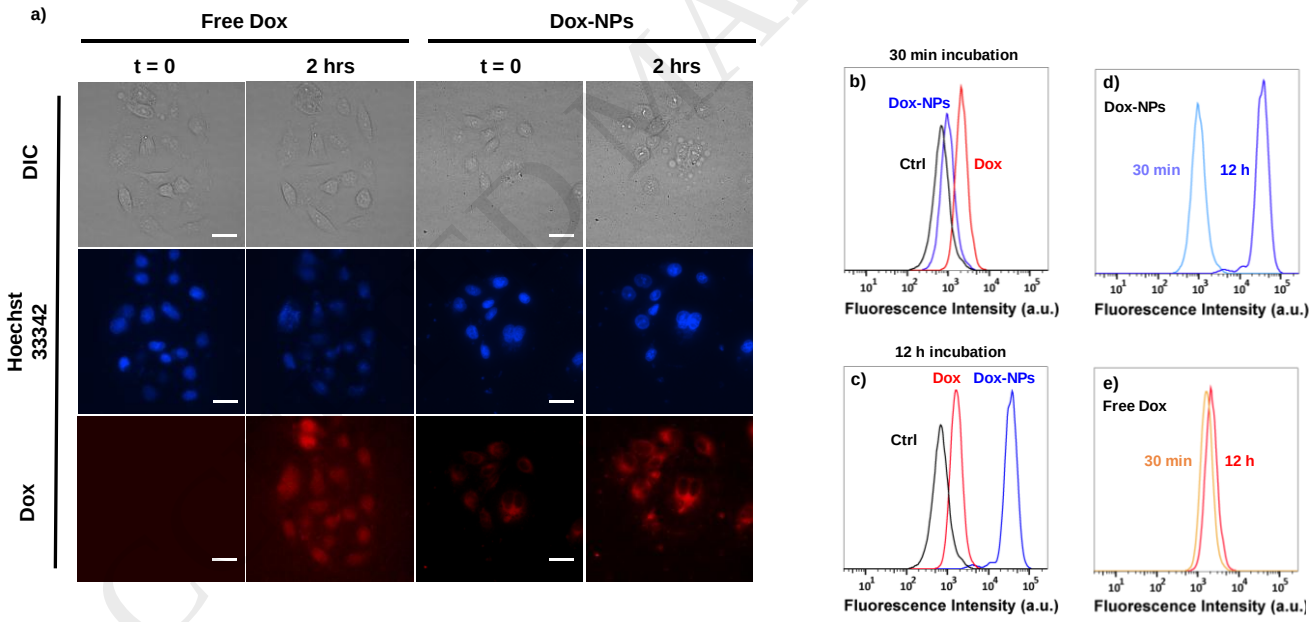

Figure 6. Time-lapse fluorescence microscopy images of HeLa cells incubated with Dox-NPs (encapsulated Dox = 1.6 µg/mL), compared with free Dox (2.5 µg/mL), for 2 hrs (a) as well as their histograms from flow cytometry after 30 min (b) and 12 hrs (c) of incubation and their comparison of free Dox-NPs (d) and Dox (e) over incubation time. Note that the images in red color (Dox) were processed differently for free Dox and Dox-NPs due to low signal from free Dox and the high signal from Dox-NPs. For all experiments, the amount of Dox-NPs was designed to have the encapsulated Dox whose concentration was kept to be 2.5 µg/mL. (Scale bar = 30 µm).

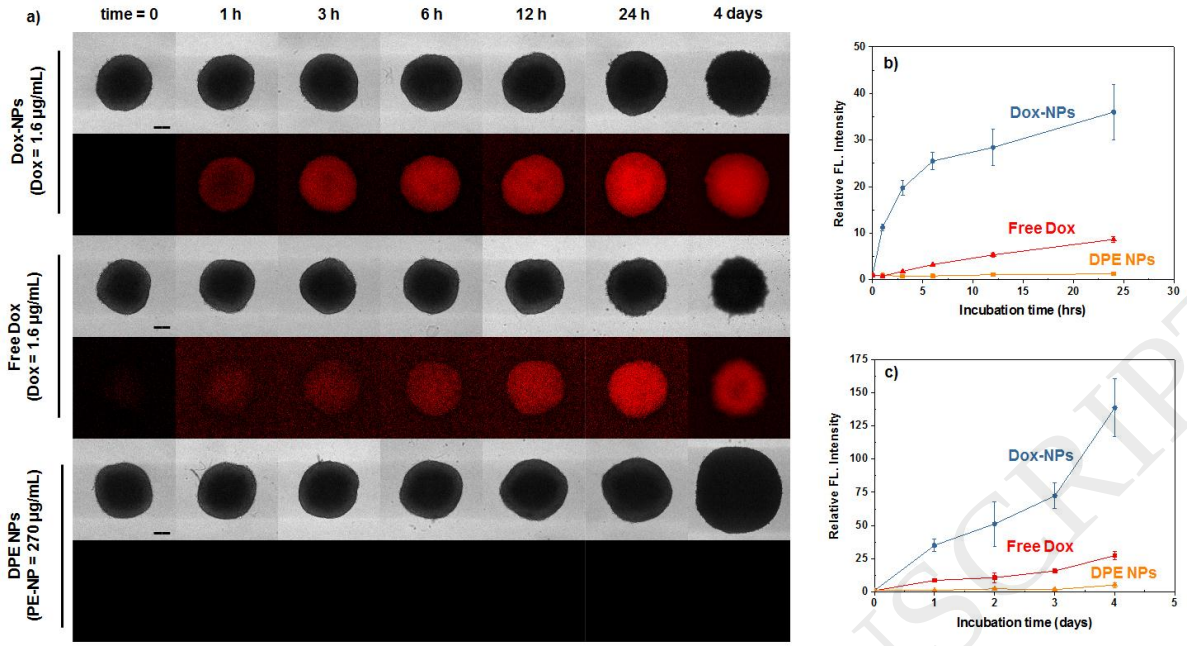

Figure 7. Florescence microscope images of HeLa spheroids incubated for 4 days with Dox NPs (encapsulated Dox = 1.6 µg/mL), free Dox (1.6 µg/mL), and empty DPE-NPs (270 µg/mL) as a control (a). Quantitative analysis of florescence intensity of the spheroids after short term (24 hrs) (b) and long term (4 days) treatments (c). Each value was normalized by their initial value. *Note that the images were processed differently for free Dox and Dox-NPs due to low signal from free Dox and high signal from Dox-NPs. (n = 3, scale bar = 200 µm).

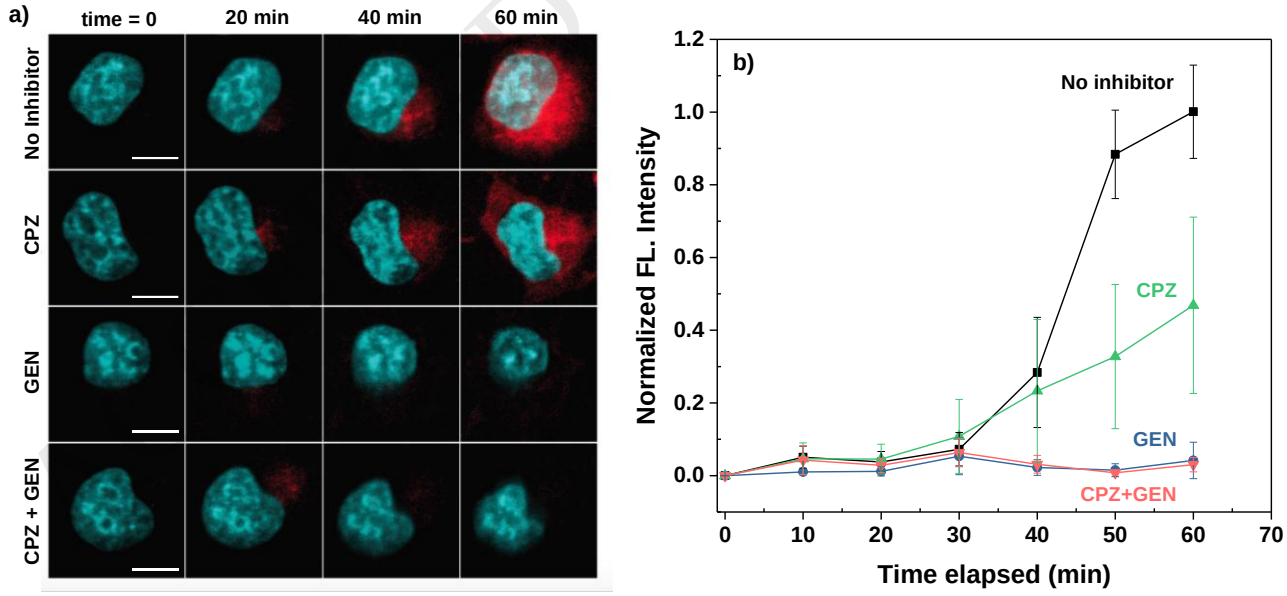

Figure 8. FL images of single cell incubated with Dox-NPs in the absence (control) and presence of chlorpromazine (CPZ, inhibiting clathrin-mediated endocytosis), or genistein (GEN, inhibiting caveolae-mediated endocytosis), or both inhibitors (a) and quantitative analysis of FL intensity of Dox in the perinuclear region normalized with maximum FL intensity of control system (no inhibitors) over 1 hr (b) (scale bar = 10 µm)